RSC Sustainability

ROYAL SOCIETY OF CHEMISTRY

PAPER

View Article Online
View Journal | View Issue

Cite this: *RSC Sustainability*, 2024, **2**, 3888

Controlling the nanoparticle size and shape of a Pt/TiO_2 catalyst for enhanced hydrogenation of furfural to furfuryl alcohol†

Heba Alsharif,[ab] Matthew B. Conway, [a] David J. Morgan, [a] Thomas E. Davies,[a] Stuart H. Taylor [a] and Meenakshisundaram Sankar *[a]

We report the selective liquid phase hydrogenation of furfural to 2-furfuryl alcohol using a Pt/TiO_2 catalyst prepared by the wet-impregnation method under mild reaction conditions (30 °C and 3 bar H_2 pressure). The effect of heat treatment protocols on the catalyst structures and the resultant catalytic properties of 4.2%Pt/TiO_2 and 0.6%Pt/TiO_2 was investigated. For both Pt loadings, the calcined + reduced catalyst exhibited higher activity compared to the reduced only catalyst, with the difference in activity being more pronounced for 4.2%Pt/TiO_2 than for 0.6%Pt/TiO_2. For the 4.2%Pt/TiO_2 catalyst, the reduced-only sample achieved 25% conversion with 90% selectivity for 2-furfuryl alcohol after 6 hours, while the calcined + reduced sample reached 99% conversion with 59% selectivity under identical reaction conditions. For the 0.6%Pt/TiO_2 catalyst, the reduced-only sample showed 70% conversion with 96% selectivity for 2-furfuryl alcohol, whereas the calcined + reduced sample achieved 97% conversion and 95% selectivity after a 2-h reaction. Characterisation of the samples using X-ray photoelectron spectroscopy, CO chemisorption and scanning transmission electron microscopy revealed that direct high temperature reduction resulted in a mixture of large Pt particles (>5 nm) with irregular shapes, small Pt nanoparticles (*ca.* 2 nm) and some sub-nm clusters. In contrast, calcination + reduction produced uniformly distributed Pt nanoparticles (*ca.* 2 nm) for both Pt loadings. Despite the presence of strong metal support interaction (SMSI) in Pt/TiO_2 catalysts, no spectroscopic evidence for such a strong interaction was found in this study. Therefore, the observed difference in catalytic activity is attributed to the variations in the shapes and sizes of the Pt nanoparticles. During the synthesis of Pt/TiO_2 catalysts, the calcination + reduction activation procedure is more beneficial for enhancing both activity and selectivity compared to a reduction only procedure.

Received 17th July 2024
Accepted 3rd September 2024

DOI: 10.1039/d4su00388h

rsc.li/rscsus

Sustainability spotlight

To realise the NetZero goals and achieve a carbon-neutral society it is crucial to develop technologies to produce chemicals and fuels from renewable feedstock. Lignocellulosic (waste) biomass is an important alternative to the conventionally used fossil-fuel based feedstock to produce chemicals and fuel molecules. Catalysis plays a central role in this endeavour by reducing the temperature of the reaction and producing the desired compound selectively. Furfuraldehyde, derived from hemicellulose, is one of the potential biomass derived compounds that could replace fossil fuel derived platform molecules. This article reports strategies to enhance the activity of Pt/TiO_2-based heterogeneous catalysts for the selective hydrogenation of furfural to furfuryl alcohol. Furfuryl alcohol is used as a monomer for producing polymers, fuel additives, dispersing agents and many more. Hence it is an important chemical in chemical and fuel production. This article targets the following UN SDGs: Affordable and Clean Energy (SDG 7), Industry, Innovation, and Infrastructure (SDG 9) and Climate Action (SDG 13).

Introduction

The conversion of lignocellulosic biomass-derived platform molecules to replace fossil fuel-based feedstocks for producing chemicals and fuel components has gained significant attention due to the global effort to achieve NetZero emissions by 2050.[1–3] The US Department of Energy (DoE) has identified furfural (FF), derived from hemicellulose, as one of the 12 potential platform molecules capable of replacing fossil fuel-based feedstocks for chemical and fuel production.[4] FF is produced in excellent yields by dehydrating xylose using ionic liquids or other acidic catalysts.[5–7] It can be converted into several industrially important chemicals through oxidation, hydrogenation and hydrogenolysis reactions.[5,8,9] Catalytic hydrogenation of FF yields various industrially significant compounds, such as tetrahydro furan (THF), tetrahydro furfuryl

[a]*Cardiff Catalysis Institute, Translational Research Hub, School of Chemistry, Cardiff University, Cardiff, CF24 4HQ, UK. E-mail: sankar@cardiff.ac.uk*

[b]*Chemistry Department, Faculty of Science, Taibah University, 41477, Al-Madinah Al-Munawarah, Saudi Arabia*

† Electronic supplementary information (ESI) available. See DOI: https://doi.org/10.1039/d4su00388h

alcohol (2-THFA),[10] 2-methyl furan (2-MF),[11] and furfuryl alcohol (2-FFA),[12] among others, as illustrated in Scheme 1. Among these compounds, 2-FFA is particularly valuable due to its diverse industrial applications, including its use as a monomer for furanic resins, a fuel component, and a dispersing agent.[13,14] Furthermore, 2-FFA can be fully hydrogenated to tetrahydrofurfuryl alcohol (2-THFFA), an environmentally benign, biodegradable green solvent. The hydrodeoxygenation of 2-FFA produces 2-methyl furan (2-MF), which serves as a fuel additive.[15,16] Therefore, developing an active heterogeneous catalyst for the selective hydrogenation of FF to 2-FFA is highly attractive from both industrial and academic perspectives.[13]

The hydrogenation of FF results in several products, which can potentially reduce the selectivity to 2-FFA. Other possible side reactions include hydrogenation of the C=C bond, hydrogenolysis (hydrodeoxygenation), ring opening and decarbonylation reactions (Scheme 1).[13,14,17] Consequently, designing catalysts for the selective conversion of FF to 2-FFA is challenging. Industrial production of 2-FFA involves the reduction of FF over a copper chromite catalyst at 180 °C and 70 to 100 bar of H_2.[18,19] However, during this reaction, the chromite catalyst converts to chromate which is toxic and harmful to the environment.[18] Therefore, research efforts should focus on developing environmentally benign catalysts that are active and selective under mild reaction conditions. Although gas-phase hydrogenation[20] and transfer hydrogenation[21] have been reported for this transformation, catalytic hydrogenation using gaseous hydrogen under mild reaction conditions is highly desirable for the sustainable production of 2-FFA.[22] These reactions are carried out at high temperatures (*ca.* 200 °C), in contrast to the ambient reaction condition reactions pursued in this work.

The nature of the metal, support, metal particle size, solvent, and reaction conditions, such as temperature, pressure, and catalyst concentration, influences the activity and selectivity of this reaction.[23] For example, polar solvents have been reported to significantly improve the rate of the FF hydrogenation reaction, although they also promote the formation of acetyl and/or ester compounds. Dichloromethane, on the other hand, has been reported to promote the hydrodeoxygenation of FF to 2-MF.[24–27] Wang *et al.* reported that higher H_2 pressure favoured the hydrogenation of FF to 2-FFA, while lower pressure favoured the hydrogenolysis of FF to furan (F) over a supported Pt catalyst.[28] Supported Pd catalysts favoured the complete hydrogenation of FF to tetrahydrofurfuryl alcohol instead of 2-FFA, whereas supported Pt catalysts favoured the formation of 2-FFA.[24,27]

Pt/TiO_2 has been reported as an effective catalyst for the selective hydrogenation of FF to 2-FFA and is extensively studied for its strong metal support interaction (SMSI).[29,30] SMSI is beneficial due to the electron rich metal-support interfacial sites and the oxygen vacancies on the TiO_2 surface.[31,32] This SMSI effect can be tuned by employing different heat treatment protocols during catalyst syntheses. Corma *et al.* reported that reducing $0.2\%Pt/TiO_2$ at 450 °C results in a TiO_2 overlayer over Pt nanoparticles (SMSI); this catalyst was found to be chemoselective (93% selectivity) whereas $0.2\%Pt/TiO_2$ without any SMSI is found to be less chemoselective (42% selectivity) during the hydrogenation of 3-nitrostyrene to 3-aminostyrene.[31] Recently, we reported a high temperature (450 °C) reduction-only treatment of the $0.5\%Pt/TiO_2$ catalyst which resulted in substantial coverage of the Pt nanoparticles by a TiO_2 overlayer, making it less active for the chemoselective hydrogenation of 3-nitrostyrene to 3-vinylaniline. However, when $0.5\%Pt/TiO_2$ was calcined and reduced at 450 °C, the TiO_2 coverage was much

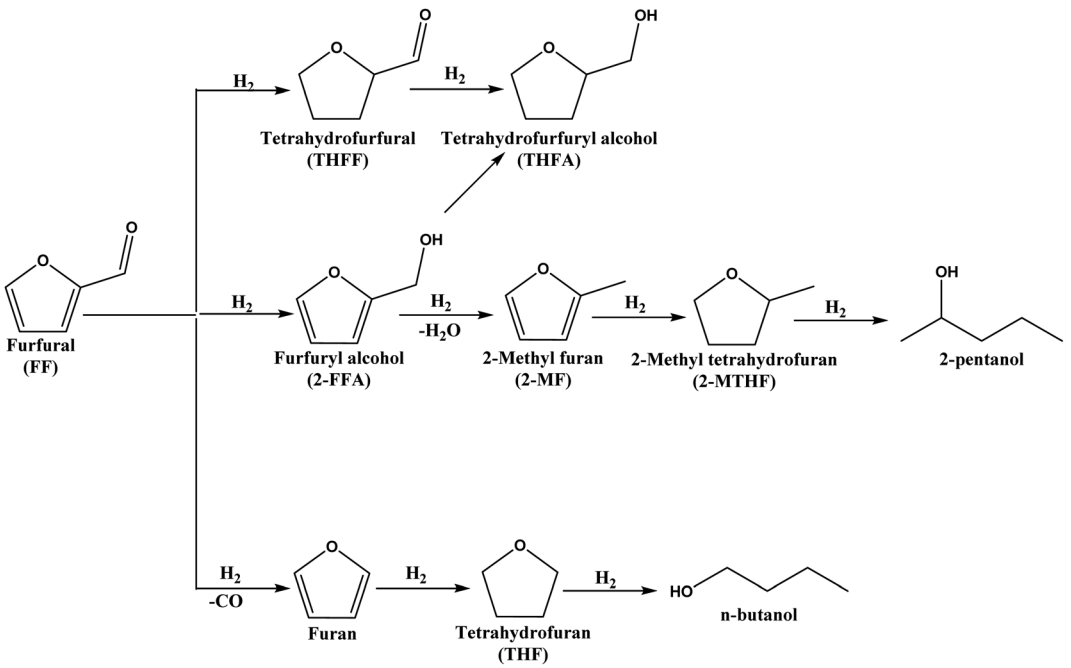

Scheme 1 Schematic representation of the various products formed from the hydrogenation of furfural.

lower, and the catalyst was much more active.[33] These examples illustrate that SMSI can be either beneficial or detrimental to the catalytic properties of Pt/TiO_2. Several groups have reported a size dependent SMSI effect for Pt/TiO_2 and Au/TiO_2 catalysts.[29,34] In supported metal catalysts, high temperature reduction increases the metal particle size and reduced catalytic activity.[35] Therefore, understanding the relationship between heat treatment protocols, structural properties and catalytic properties is crucial. This work aims to understand the relationship between heat treatment protocols and the catalytic properties of Pt/TiO_2 for the selective hydrogenation of FF to 2-FFA under mild reaction conditions.

Experimental

Materials and methods

All the chemicals used in this work were purchased from commercial sources and were used without any further purification: $H_2PtCl_6 \cdot 6H_2O$ (Sigma-Aldrich, ≥37.50% Pt basis), titania P25 (99.9%, Degussa), furfural (99%, Sigma-Aldrich), furfuryl alcohol (98%, Sigma-Aldrich) and isopropanol (99.5%, Fisher Scientific).

Catalyst preparation. All supported metal catalysts used in this work were prepared *via* the wet-impregnation methodology.[33] In a typical catalyst synthesis, a 50-mL round bottom flask equipped with a magnetic stirrer bar was charged with the required quantity of the aqueous metal precursor solution ($H_2PtCl_6 \cdot 6H_2O$ (18.57 mg_{Pt} mL^{-1})) and distilled water to achieve a total volume of 16 mL. After heating the round bottom flask at 60 °C for 10 minutes, the requisite amount of the support was slowly added. After the complete addition of the support, the slurry was stirred for another 15 minutes. Then the temperature was increased to 95 °C and the stirring of the slurry was continued. The flask was left at 95 °C for 16 h to facilitate gradual evaporation of water. Finally, the dry solid mixture was thoroughly ground into a fine powder using a pestle and mortar. This sample was labelled as the dried-only sample. This dried-only sample was subjected to different heating protocols to generate the calcined only (C), reduced only (R) and calcination followed by reduction (C + R) catalysts. The calcined only catalyst was obtained by calcining 1 g of the dried-only material in a furnace at 450 °C with a ramp rate of 10 °C min^{-1} for 4 h under flowing air. The reduced only sample was obtained by reducing 1 g of the dried-only sample under a flow of 5% H_2/Ar at 450 °C with a ramp rate of 10 °C min^{-1} for 4 h. The calcined and reduced sample was obtained by calcining the dried-only sample in a furnace at 450 °C for 4 h under flowing air; then the furnace was cooled to 25 °C, and then the sample was reduced under a flow of 5% H_2/Ar at 450 °C for 4 h. The catalyst synthesis conditions, including the calcination and reduction temperatures are chosen based on the results presented in our previous work.[33]

Catalytic testing

Liquid phase hydrogenation of furfural. Hydrogenation of FF was performed in a 50 mL moderate pressure batch glass reactor under 3 bar H_2 pressure. The reactor was loaded with 4.45 mmol of FF, an appropriate amount of catalyst ($mol_{FF}/mol_{metal} = 207$) and 15 mL of isopropanol. The glass reactor was sealed, purged with gaseous N_2 three times, and then purged with H_2 three times before it was pressurised with H_2 to 3 bar. The H_2 inlet line was kept open throughout the reaction to replenish the consumed H_2. The experiment was performed at 30 °C, and the reaction mixture was continuously stirred at 800 rpm with a magnetic stirrer. At the end of the reaction, the reactor was cooled in an ice bath for 10 minutes, and the catalyst was separated from the reaction mixture using a 0.45 μm PTFE syringe filter. An aliquot was removed from the filtered reaction mixture for gas chromatography (GC) analysis. The GC sample was prepared by mixing 10 mL of the reaction mixture with 0.1 mL of *n*-octanol (external standard). 1 mL of this mixture was analysed. Quantitative analyses of the reaction mixtures were conducted using a Bruker scion 456 GC fitted with a RESTEK Rtx@-1 (60 m, 0.32 mm ID) column and an FID detector. N_2 was used as the carrier gas. Quantitative analyses used an external standard (*n*-octanol) and response factors derived from calibration mixtures. The stability and reusability of the catalyst were investigated under the same reaction conditions (3 h, 30 °C, 3 bar H_2). After every reaction cycle, the solid catalyst was removed from the reaction mixture using a centrifuge and washed thoroughly using isopropanol and acetone twice. The catalyst was then dried under ambient conditions before using it for the next cycle.

$$\text{FF conversion}(\%) = \left(\frac{\text{FF concentration}(0) - \text{FF concentration }(t)}{\text{FF concentration }(0)}\right) \times 100$$

$$\text{2FFA selectivity}(\%) = \left(\frac{\text{2FFA concentration}}{\text{Sum of concentrations of all the products}}\right) \times 100$$

Catalyst characterisation

X-ray photoelectron spectroscopy (XPS). The surface chemistry of the catalysts was investigated using X-ray photoelectron spectroscopy (XPS). All measurements were performed on a Kratos Axis Ultra DLD photoelectron spectrometer, using monochromatic Al radiation operating at 144 W (12 mA × 12 kV). The samples were mounted by pressing onto Scotch 665 double sided adhesive tape mounted on a standard Kratos sample bar. The samples were evacuated from the atmosphere to *ca.* 10^{-8} mbar, before transfer to the analysis chamber. Data were acquired using the hybrid mode with the slot aperture, yielding an analysis area of approximately 700 × 300 microns. Charge compensation was achieved using low energy electrons. Whilst charge correction is typically made to the C(1s) line of adventitious carbon, it was found to be unstable for these materials, given the various oxidative and reductive treatments, and hence the resulting spectra were calibrated to the Ti($2p_{3/2}$) line of the titania support and taken to be 458.5 eV. All data were analysed using CasaXPS,[17] following the removal of a Shirley

type background. Atomic percentages were calculated using modified Wagner sensitivity factors as supplied by the instrument manufacturer.

Scanning transmission electron microscopy (STEM). STEM analysis was conducted on a probe corrected ThermoFisher Scientific Spectra 200 operating at 200 kV. The beam current was 30–100 pA with a convergence angle of 21.5 mrad. The samples were deposited by dry dispersion onto 300 mesh copper grids coated with a holey carbon film.

CO chemisorption. CO chemisorption was conducted using a Micromeritics AutoChem II 2920 instrument equipped with a thermal conductivity detector (TCD). The Pt/TiO_2 samples were inserted into a quartz u-tube between two pieces of quartz wool and pre-treated in a 10% H_2/Ar flow (50 mL min^{-1}) for 1 h at 300 °C (10 °C min^{-1} ramp). Subsequently, the gas flow was changed to Ar (50 mL min^{-1}) while the temperature was fixed at 300 °C to purge the system of residual H_2 for 1 h. The sample was then cooled to 35 °C and the gas flow was switched to He (50 mL min^{-1}). The TCD baseline was allowed to stabilise and pulses of 1% CO/He were injected until peak areas remained constant. Particle property information (dispersion, particle size and metal surface area) was obtained following literature procedures.[36] The dispersion (D) stoichiometry of CO/Pt was assumed to be 1. The particle size was calculated using the equation d (nm) = 1.12/D. The platinum surface area was calculated according to the equation surface area ($m^2\ g_{Pt}^{-1}$) = 249.12D.

Results and discussion

Catalyst testing

Heat treatment during catalyst synthesis plays a crucial role in determining the structural properties of Pt/TiO_2 catalysts, particularly regarding the extent of strong metal support interactions (SMSIs), metal particle sizes and nanostructures. SMSI in Pt/TiO_2 has been reported to significantly impact catalytic activity, selectivity and stability in various reactions, including hydrogenation of nitroarenes,[31] CO_2 hydrogenation,[37] and propane dehydrogenation.[38] Recently, we reported how heat treatment protocols tune the Pt loading-dependent SMSI on Pt/TiO_2 and its effect on the chemoselective hydrogenation of 3-nitrostyrene.[33] Similarly, heat treatment protocols play a crucial role in the catalytic activities of Pt/TiO_2 during CO oxidation, photocatalytic alcohol oxidation and hydrogen evolution reactions.[39–41] To study the relationship between Pt loading, heat treatment and the catalytic properties of Pt/TiO_2 for the chemoselective hydrogenation of FF, we prepared 4.2 wt% Pt/TiO_2 catalysts using the wet-impregnation method. The dried only catalyst was either reduced at 450 °C (R), calcined at 450 °C (C) or calcined at 450 °C followed by reduction at 450 °C for 4 h (C + R). To study the effect of catalyst heat treatment on FF hydrogenation activity, we tested 4.2%Pt/TiO_2 (C), 4.2%Pt/TiO_2 (R) and 4.2%Pt/TiO_2 (C + R) materials. The results (Fig. 1a) show that 4.2%Pt/TiO_2 (R) is the least active catalyst, with *ca.* 25% conversion with 90% selectivity to 2-FFA after 6 h. The 4.2%Pt/TiO_2 (C) catalyst showed 90% conversion and 42% selectivity. However, the 4.2%Pt/TiO_2 (C + R) catalyst exhibited the highest conversion (*ca.* 99%) with 59% selectivity to 2-FFA. Fig. 1 shows the selectivity data for 2-FFA only. A detailed selectivity profile is provided in Table S1 (ESI).†

When alcohols are used as solvents in this reaction, FF and 2-FFA undergo acetylation, resulting in products referred to as solvent products in this article (ESI, Scheme S1†).[27] However, these solvent products are formed in lower quantities (>5%). These reactions are catalyzed by the acidic sites on the TiO_2 support. Numerous studies have quantified the acidic sites on the TiO_2 material used in this research.[42] The catalytic performance as a function of the reaction time for 4.2%Pt/TiO_2 (R) and 4.2%Pt/TiO_2 (C + R) shows a clear difference in the activity and selectivity between them (ESI, Fig. S1†). The lowest activity for 4.2%Pt/TiO_2 (R) could be because of two reasons: (a) SMSI leading to loss of Pt surface atoms and (b) large Pt particle size because of high temperature reduction. Both phenomena have been reported during high temperature reduction of supported Pt nanoparticles.[30,32,34,38,41] The difference in 2-FFA selectivity between 4.2%Pt/TiO_2 (C) and 4.2%Pt/TiO_2 (R) catalysts suggests

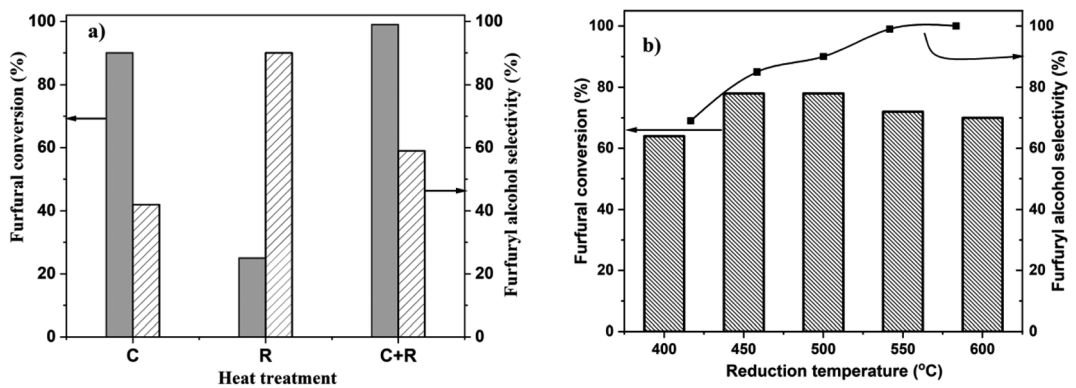

Fig. 1 Effect of heat treatment on 4.2%Pt/TiO_2 for the liquid phase hydrogenation of furfural to furfuryl alcohol: (a) calcined-only (C) *vs.* reduction-only (R) *vs.* calcination + reduction (C + R) at 450 °C, time: 6 h; (b) catalytic data of 4.2%Pt/TiO_2 calcined at 450 °C followed by reduction at different temperatures. Reaction conditions: FF: 4.45 mmol; i-PrOH: 15 mL; temp: 30 °C; H_2: 3 bar; substrate/metal molar ratio = 207; time: 3 h.

that the Pt oxidation state plays an important role in the catalytic properties. Since 4.2%Pt/TiO_2 (C + R) is the most active and selective catalyst for this reaction, C + R treatment was performed for all the other samples.

To study the effect of reduction temperature, the dried only catalyst was calcined at 450 °C and then reduced at different temperatures ranging from 400 °C to 600 °C. The catalytic results for all these materials are presented in Fig. 1b. 4.2%Pt/TiO_2 (C + R) – 450 °C showed the highest FF conversion (78%) with 87% selectivity to 2-FFA. The 4.2%Pt/TiO_2 (C + R) – 600 °C catalyst showed the highest 2-FFA selectivity (98%) but with a lower conversion (70%). The data presented in Fig. 2b show that the 2-FFA selectivity increases with an increase in the catalyst reduction temperature; however, the conversion is the highest for the catalyst reduced at 450 °C and 500 °C. All these results clearly show that heat treatment has a significant impact on the catalytic properties (activity and selectivity) of 4.2%Pt/TiO_2 for the chemoselective hydrogenation of FF to 2-FFA.

Pt loading on the support influences the particle size and the extent of SMSI, and hence the catalytic properties.[29,33] To study this in detail, Pt/TiO_2 catalysts, with four different Pt loadings (4.2 wt%, 2.4 wt%, 1.4 wt% and 0.6 wt%) were synthesized and calcined at 450 °C and reduced (C + R) at 450 °C for 4 h. All these catalysts were tested for the hydrogenation of FF and the results are presented in Fig. 2a. The corresponding catalytic performance as a function of the reaction time is presented in the ESI (Fig. S2–S4).† To normalize different Pt loadings, the catalyst masses were varied to maintain a constant FF : Pt molar ratio of 207. The catalytic data clearly show that the conversion increases substantially with the reduction in the Pt loading. 0.6% Pt shows the highest catalytic activity among all the catalysts tested. The conversion and selectivity for the catalysts with different Pt loadings followed the same trend – 4.2%Pt/TiO_2 (50% conversion & 67% selectivity) < 2.4%Pt/TiO_2 (71% conversion & 86% selectivity) < 1.4%Pt/TiO_2 (71% conversion & 89% selectivity) < 0.6%Pt/TiO_2 (81% conversion with 95% selectivity) after 2 h reaction time. The activities of 2.4%Pt/TiO_2 and 1.4%Pt/TiO_2 are similar suggesting that their structural features, most likely Pt particle sizes, are similar.

The effect of heat treatment (R *vs.* C + R) on the catalytic properties of the most active 0.6%Pt/TiO_2 catalyst was investigated and the results are presented in Fig. 2b. Similar to the 4.2%Pt/TiO_2 catalyst, the 0.6%Pt/TiO_2 (C + R) catalyst is more active (97% conversion) than 0.6%Pt/TiO_2 (R) (70% conversion) with the same 2-FFA selectivity (*ca.* 95%). However, the difference in catalytic activity between the two heat treated samples is much smaller for the 0.6%Pt/TiO_2 catalyst (27%) compared to the 4.2%Pt/TiO_2 catalyst (74%). This suggests that the extent of the role of heat treatment in the structural features of Pt/TiO_2 depends on Pt loading. The catalytic performance data as a function of the reaction time of the 0.6%Pt/TiO_2 catalyst (Fig. 2b) show a higher rate of FF conversion for the first 2 h (80% conversion) followed by a slower rate regime to reach >98% conversion after 6 h. Initially, the reaction was highly selective to 2-FFA (100% after 1 h); however, the selectivity decreased slightly with time (95% after 6 h). This reduction in selectivity is due to the formation of an acetylation product (ESI Scheme S1†). Among the catalysts tested in this work, 0.6%Pt/TiO_2 (C + R) is the most active catalyst for the liquid phase chemoselective hydrogenation of FF to 2-FFA at 30 °C and is also one of the most active catalysts reported for this transformation (ESI, S3†).

Catalyst stability during the reaction and its reusability for subsequent reactions are crucial for heterogeneous catalysts. Reusability of the 0.6%Pt/TiO_2 (C + R) catalyst was tested and the results are presented in Fig. 3.

0.6%Pt/TiO_2 lost activity during reuse, decreasing from 90% conversion for the fresh catalyst to 35% conversion during the 3rd recycle. The 2-FFA selectivity also reduced from 95% to 51% during the 3rd recycle. There is a clear deactivation of this catalyst. Preliminary studies of the deactivated samples suggest that the deactivation is due to the sintering of particles and there is no leaching of Pt. However, detailed investigation is needed.

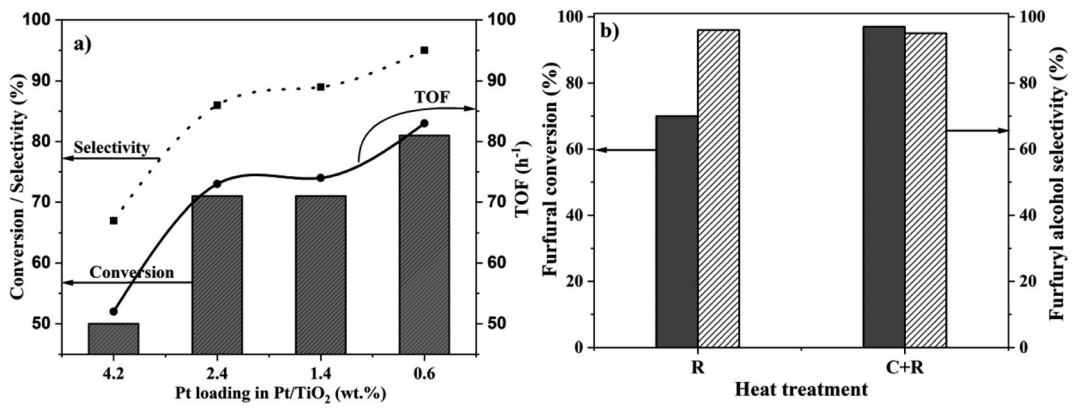

Fig. 2 (a) Effect of Pt loading on the catalytic activity for the liquid-phase hydrogenation of FF. Reaction conditions: FF: 4.45 mmol; i-PrOH: 15 mL; temp: 30 °C; H_2: 3 bar; substrate/metal molar ratio = 207; time: 2 h. (b) Comparison of the catalytic data of 0.6%Pt/TiO_2 (C + R) and 0.6%Pt/TiO_2 (R) for the liquid phase hydrogenation of FF. Reaction conditions: FF: 4.45 mmol; i-PrOH: 15 mL; temp: 30 °C; H2: 3 bar; substrate/metal molar ratio = 207.

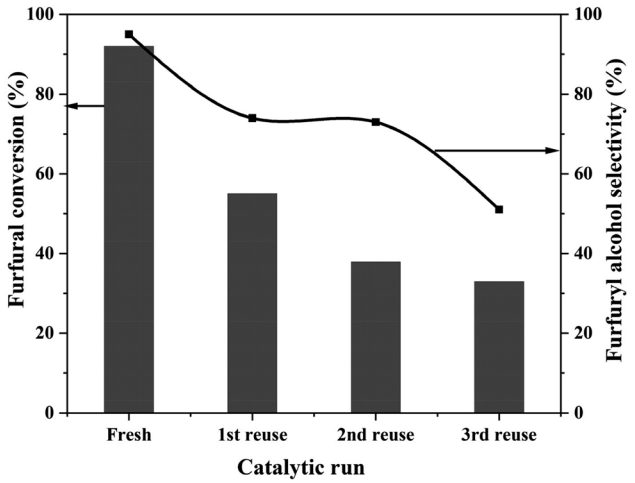

Fig. 3 Reusability of the 0.6%Pt/TiO_2 (C + R) catalyst. Reaction conditions: FF: 4.45 mmol; i-PrOH: 15 mL; temp: 30 °C; H_2: 3 bar; substrate/metal molar ratio = 207; time: 3 h.

Catalyst characterisation

To understand the relationship between the observed catalytic behaviour, heat treatment protocols and metal loading, all the catalysts were characterized by XPS, TEM and CO chemisorption.

To understand the effect of heat treatment protocols and Pt loading on the valence states, the dried only, reduced only and calcined + reduced materials were characterized by XPS (Fig. 4). The dried 4.2%Pt/TiO_2 catalyst (Fig. 4d) revealed two Pt species; the first at 72.7 eV corresponding to Pt^{2+} in $Pt(OH)_2$, whilst the peak at 74.7 eV is assigned to $PtCl_x$ species, and supported by a significant corresponding chlorine signal (not shown). Calcination (Fig. 4c) reduces the total chloride content; however, some Pt–Cl species remain on the sample surface. Reductive treatment at 450 °C reveals the characteristic asymmetric shape of metallic $Pt^0(4f_{7/2})$ centered at 70.5 eV (Fig. 4b). For the calcined + reduced sample the $Pt^0(4f_{7/2})$ binding energy is slightly higher at 70.9 eV (Fig. 4a), and is expected for bulk metallic Pt, and this indicates the absence of a strong interaction between Pt and TiO_2. The reduced only sample shows a high negative BE shift (*ca.* 0.4 eV) compared to the calcined + reduced sample. A strong electronic interaction between TiO_2 and Pt or a large increase in the Pt metal particle size for the reduced only sample can explain this negative BE shift. A strong interaction between TiO_2 and Pt results in the transfer of electrons from Ti^{3+} to Pt and can result in a negative shift of the $Pt^0(4f_{7/2})$ BE for the reduced only sample.[29] Another interpretation could be the presence of large Pt nanoparticles in the reduced-only sample resulting in a negative BE shift because of the relaxation shift.[43] For the 0.6%Pt/TiO_2 sample, there is no

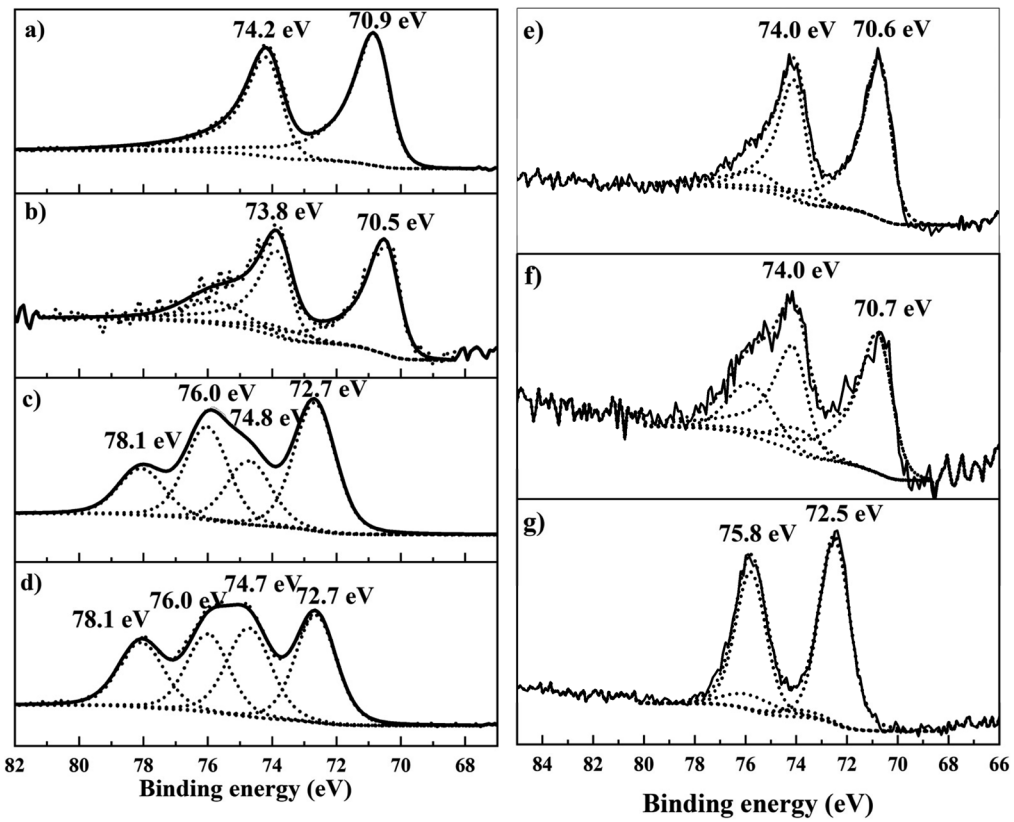

Fig. 4 Pt 4f core-level spectra of 4.2%Pt/TiO_2 (C + R) (a); 4.2%Pt/TiO_2 (R) (b); 4.2%Pt/TiO_2 (C) (c); 4.2%Pt/TiO_2 dried (d); 0.6%Pt/TiO_2 (C + R) (e); 0.6%Pt/TiO_2 (R) (f); and 0.6%Pt/TiO_2 dried (g) samples. For the lower Pt concentrations, the Ti loss structure is evident in the range *ca.* 73–77 eV in the spectra (b and e–g).

Table 1 CO chemisorption and Pt surface concentration data for the supported Pt/TiO_2 catalysts

Catalyst	CO uptake mmol g^{-1}	Dispersion (%)	Surface area (m^2 g_{Pt}^{-1})	Pt surface concentration[a]
0.6%Pt/TiO_2 (R)	0.00822	27	66	0.15
0.6%Pt/TiO_2 (C + R)	0.0264	86	210	0.24
4.2%Pt/TiO_2 (R)	0.00963	4	11	0.14
4.2%Pt/TiO_2 (C + R)	0.0958	44	110	1.24

[a] Calculated from the XPS data presented in Fig. 4.

difference in the Pt^0 ($4f_{7/2}$) binding energies between the reduced only and calcined + reduced samples (70.6 eV for the reduced only sample and 70.7 eV for the calcined + reduced sample). The XPS data clearly indicate the difference in Pt valence states for the reduced only and calcined + reduced samples of 4.2%Pt/TiO_2 catalysts. However, no such difference in BE is observed for the 0.6%Pt/TiO_2 sample and this matches the catalytic activity trend observed for these catalysts. A detailed BE assignment is provided in the ESI (Table S2).† To investigate the reason behind the negative shift in BE between the reduced only and the calcined + reduced samples of the Pt/TiO_2 catalysts, they were characterised by CO chemisorption (Table 1).

For both loadings, the reduced only sample has a lower Pt surface area compared to the calcined + reduced samples. However, the difference between them is more pronounced in the 4.2%Pt/TiO_2 catalyst; the calcined + reduced sample has 10-fold more Pt surface area compared to the reduced only sample. However, for the 0.6%Pt/TiO_2 catalyst, the calcined + reduced sample has *ca.* 3-fold more Pt surface area compared to the reduced only sample. This trend matches well with the observed catalytic trend for all these samples. Either Pt particle size changes or the extent of TiO_x covering the Pt surface (typically called SMSI) can influence the Pt surface area derived from CO chemisorption measurements.

Selected Pt/TiO_2 samples were characterized by scanning transmission electron microscopy (STEM) to assess the Pt particle size distribution (Fig. 5 and 6). The 4.2%Pt/TiO_2 (C + R) sample (Fig. 5a) displays a narrow particle size distribution with most of the particles being disordered finite aggregates of atoms in the range of *ca.* 1–2 nm (Fig. 5a(ii) and (iii)). Several sub-nm Pt clusters and single atoms of Pt can also be seen (Fig. 5a(i)). On the other hand, the 4.2%Pt/TiO_2 (R) sample has a heterogeneous distribution of Pt particles (Fig. 5b). A large proportion of the particles are coral-like structures (>50 nm) with irregular shapes with a smaller number present as faceted nanoparticles with diameters of approximately 1–5 nm (Fig. 5b(ii)). This clearly indicates that the observed negative shift in BE for the $Pt^0(4f_{7/2})$ peak is due to large (>5 nm) Pt nanoparticles and not because of SMSI. Lattice measurements of the larger particles give a spacing of 0.236 nm consistent with the (111) plane in cubic Pt (ICDD 00-004-0802) (Fig. 5b(i)). Careful analyses of the STEM images did not provide any evidence of a TiO_x layer covering the Pt nanoparticles' surface. This rules out the possibility of a strong metal support interaction between Pt and TiO_2. Fig. S5 (ESI)† shows the lower magnification images of these samples further highlighting the presence of large Pt nanoparticles with highly irregular shapes in the reduced only samples. This is consistent with the CO chemisorption data. The observed difference in catalytic activity between 4.2%Pt/TiO_2 (R) and 4.2%Pt/TiO_2 (C + R) is therefore determined to be due to the clear and distinct difference in particle size and morphology. The STEM images of 0.6%Pt/TiO_2 (Fig. 6a and b) show a similar trend. 0.6%Pt/TiO_2 (C + R) (Fig. 6a) has a mixture of small Pt particles (<2 nm) and some sub-nm Pt clusters and Pt atoms (Fig. 6a(i)). However, 0.6%Pt/

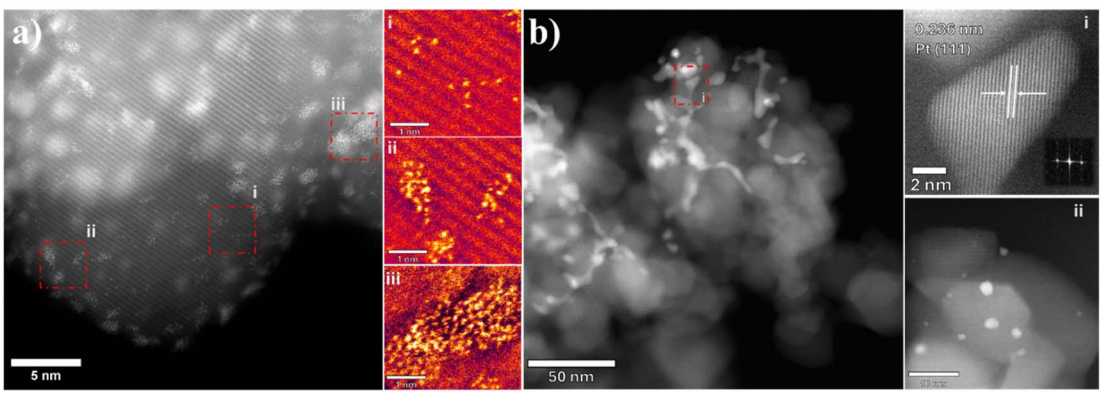

Fig. 5 Scanning transmission electron micrographs of (a) 4.2%Pt/TiO_2 (C + R) with the marked areas (i–iii) shown as high-pass filtered, coloured extracts to highlight the presence of single atoms, irregular clusters and rafts; (b) 4.2%Pt/TiO_2 (R) displaying large non-uniform corals with the marked area (i) showing the presence of Pt. Image ii shows the smaller more uniform nanoparticles also present.

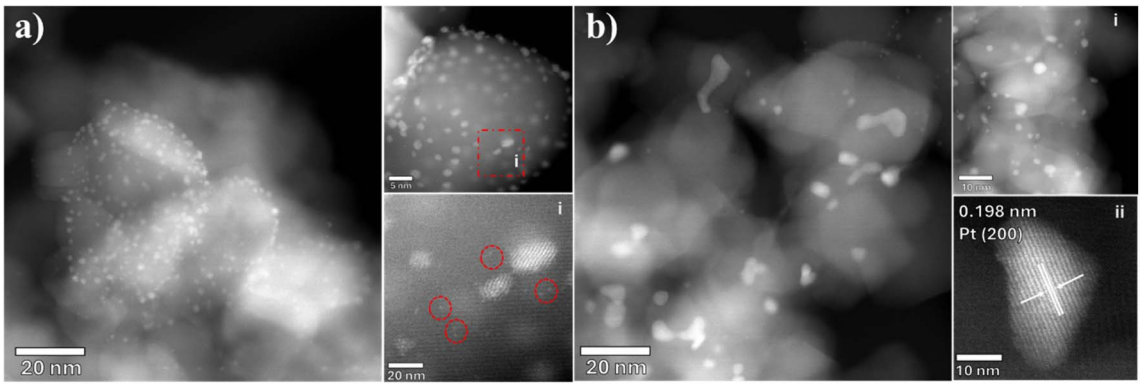

Fig. 6 Scanning transmission electron micrographs of (a) 0.6%Pt/TiO_2 (C + R) with the marked area (i) highlighting the presence of single atoms, irregular clusters and rafts and (b) 0.6%Pt/TiO_2 (R) showing the irregular particles identified as Pt in image (ii). Image (i) shows the smaller more uniform nanoparticles also present.

TiO_2 (R) shows a mixture of large Pt particles (>20 nm) with irregular shapes (Fig. 6b) and small (<2 nm) Pt particles (Fig. 6b(ii)). Again, the lattice fringe measurements determine the particle to be Pt as opposed to PtO_x (Fig. 6b(i)). This is consistent with the difference in Pt surface area (Table 1) observed for these two samples. Due to the presence of single atoms, clusters, non-uniform corals and quasi-spherical Pt particles a meaningful particle size distribution for these catalysts could not be calculated.

Preliminary investigations were conducted to understand the reason for the deactivation of the 0.6%Pt/TiO_2 catalyst. XPS spectra of the spent catalyst (after 3 runs) show no difference in the $Pt^0(4f_{7/2})$ BE compared to that of the fresh sample (ESI, Fig. S7†), suggesting no change in the oxidation state or the particle sizes of Pt in the deactivated catalyst. The Pt content of the fresh and the spent samples of 0.6%Pt/TiO_2, analysed by ICP-MS, (ESI, Table S3†) did not show any change, ruling out Pt leaching during the reaction. Preliminary low-resolution TEM analyses of the fresh and deactivated samples (ESI, Fig. S8†) did not show any major changes in the Pt particle size which aligns with the XPS results of the spent sample. As mentioned above, all these catalysts contain a heterogeneous mixture of Pt single atoms, sub-nm clusters and large nanoparticles. Hence, a meaningful particle size distribution cannot be calculated. Due to this uncertainty in the Pt particle size distribution sintering cannot be completely ruled out. Further investigation is necessary to find out the reason for catalyst deactivation.

Conclusions

Here we report that 0.6%Pt/TiO_2 calcined and reduced at 450 °C is an active and selective catalyst for the liquid phase hydrogenation of furfural to 2-furfuryl alcohol at 30 °C under 3 bar H_2. This is one of the most active catalysts reported in the literature (ESI, Table S4†). XPS, CO chemisorption and STEM characterization of this catalyst revealed small Pt particles (<2 nm) with uniform distribution, making it one of the most active catalysts reported for this transformation. For both 4.2%Pt/TiO_2 and 0.6%Pt/TiO_2 catalyst heat treatment plays a crucial role. Direct high temperature reduction at 450 °C results in a mixture of large Pt particles (>5 nm) with irregular shapes, small nanoparticles (*ca.* 2 nm) and some sub-nm clusters. STEM characterization did not provide any evidence for a strong metal support interaction (SMSI) in the reduced only samples. However, calcination followed by reduction at 450 °C results in a more uniform distribution of Pt nanoparticles. Consequently, the calcined + reduced catalysts are more active than the reduced only catalysts. The difference between the two heat treated samples is more pronounced in 4.2%Pt/TiO_2.

Data availability

The data supporting this article have been included as part of the ESI.†

Conflicts of interest

There are no conflicts to declare.

Acknowledgements

HA thanks the Kingdom of Saudi Arabia and Taibah University for funding her PhD studies. MC and MS acknowledge the funding by the Engineering and Physical Sciences Research Council *via* the Prosperity Partnership EP/V056565/1 with bp and Johnson Matthey plc in collaboration with Cardiff University and the University of Manchester. XPS data collection was performed at the EPSRC National Facility for XPS ("HarwellXPS"), operated by Cardiff University and UCL, under Contract No. PR16195. The authors would like to thank the CCI-Electron Microscopy Facility which has been partially funded by the European Regional Development Fund through the Welsh Government and The Wolfson Foundation.

References

1 G. W. Huber, S. Iborra and A. Corma, *Chem. Rev.*, 2006, **106**, 4044–4098.

2 G. Li, R. Wang, J. Pang, A. Wang, N. Li and T. Zhang, *Chem. Rev.*, 2024, **124**, 2889–2954.
3 A. S. Rathore and A. Singh, *J. Chem. Technol. Biotechnol.*, 2022, **97**, 597–607.
4 T. Werpy and G. Petersen, *Top Value Added Chemicals from Biomass, Volume I, Results of Screening for Potential Candidates from Sugar and Synthesis Gas*, US Department of Energy DOE/GO-102004-1992, 2004, **http://www.eere.energy.gov/biomass/pdfs/35523.pdf**.
5 A. Jaswal, P. P. Singh and T. Mondal, *Green Chem.*, 2022, **24**, 510–551.
6 S. Peleteiro, S. Rivas, J. L. Alonso, V. Santos and J. C. Parajó, *Bioresour. Technol.*, 2016, **202**, 181–191.
7 V. Choudhary, S. I. Sandler and D. G. Vlachos, *ACS Catal.*, 2012, **2**, 2022–2028.
8 R. Mariscal, P. Maireles-Torres, M. Ojeda, I. Sádaba and M. López Granados, *Energy Environ. Sci.*, 2016, **9**, 1144–1189.
9 X. Li, P. Jia and T. Wang, *ACS Catal.*, 2016, **6**, 7621–7640.
10 J. Wu, X. Zhang, Q. Chen, L. Chen, Q. Liu, C. Wang and L. Ma, *Energy Fuels*, 2019, **34**, 2178–2184.
11 Q. Yuan, J. Pang, W. Yu and M. Zheng, *Catalysts*, 2020, **10**(11), 1304.
12 A. C. Matsheku, M. C. Maumela and B. C. E. Makhubela, *RSC Sustainability*, 2023, **1**, 1471–1483.
13 A. Racha, C. Samanta, S. Sreekantan and B. Marimuthu, *Energy Fuels*, 2023, **37**, 11475–11496.
14 Z. An and J. Li, *Green Chem.*, 2022, **24**, 1780–1808.
15 J. Chuseang, R. Nakwachara, M. Kalong, S. Ratchahat, W. Koo-amornpattana, W. Klysubun, P. Khemthong, K. Faungnawakij, S. Assabumrungrat, V. Itthibenchapong and A. Srifa, *Sustainable Energy Fuels*, 2021, **5**, 1379–1393.
16 M. Thewes, M. Muether, S. Pischinger, M. Budde, A. Brunn, A. Sehr, P. Adomeit and J. Klankermayer, *Energy Fuels*, 2011, **25**, 5549–5561.
17 Y. Wang, D. Zhao, D. Rodríguez-Padrón and C. Len, *Catalysts*, 2019, **9**, 796.
18 Q. Yang, D. Gao, C. Li, S. Cao, S. Li, H. Zhao, C. Li, G. Zheng and G. Chen, *Fuel*, 2022, **311**, 122584.
19 F. Hao, J. Zheng, S. He, H. Zhang, P. Liu, H. Luo and W. Xiong, *Catal. Commun.*, 2021, **151**, 106266.
20 K. Vikrant and K. Kim, *Sci. Total Environ.*, 2023, **904**, 166882.
21 L. Grazia, A. Lolli, F. Folco, Y. Zhang, S. Albonetti and F. Cavani, *Catal. Sci. Technol.*, 2016, **6**, 4418.
22 X. Li, P. Jia and T. Wang, *ACS Catal.*, 2016, **6**(11), 7621.
23 Z. Yu, X. Lu, X. Wang, J. Xiong, X. Li, R. Zhang and N. Ji, *ChemSusChem*, 2020, **13**, 5185–5198.
24 R. Albilali, M. Douthwaite, Q. He and S. H. Taylor, *Catal. Sci. Technol.*, 2018, **8**, 252–267.
25 X. Gao, S. Tian, Y. Jin, X. Wan, C. Zhou, R. Chen, Y. Dai and Y. Yang, *ACS Sustain. Chem. Eng.*, 2020, **8**, 12722–12730.
26 J. Wang, C.-Q. Lv, J.-H. Liu, R.-R. Ren and G.-C. Wang, *Int. J. Hydrogen Energy*, 2021, **46**, 1592–1604.
27 M. J. Taylor, L. J. Durndell, M. A. Isaacs, C. M. A. Parlett, K. Wilson, A. F. Lee and G. Kyriakou, *Appl. Catal., B*, 2016, **180**, 580–585.
28 C. Wang, J. Luo, V. Liao, J. D. Lee, T. M. Onn, C. B. Murray and R. J. Gorte, *Catal. Today*, 2018, **302**, 73–79.
29 Z. Wu, Y. Li and W. Huang, *J. Phys. Chem. Lett.*, 2020, **11**, 4603–4607.
30 A. Beck, H. Frey, X. Huang, A. H. Clark, E. D. Goodman, M. Cargnello, M. Willinger and J. A. van Bokhoven, *Angew. Chem., Int. Ed.*, 2023, **62**, e202301468.
31 A. Corma, P. Serna, P. Concepción and J. J. Calvino, *J. Am. Chem. Soc.*, 2008, **130**, 8748–8753.
32 T. Pu, W. Zhang and M. Zhu, *Angew. Chem., Int. Ed.*, 2023, **62**, e202212278.
33 M. Macino, A. J. Barnes, S. M. Althahban, R. Qu, E. K. Gibson, D. J. Morgan, S. J. Freakley, N. Dimitratos, C. J. Kiely, X. Gao, A. M. Beale, D. Bethell, Q. He, M. Sankar and G. J. Hutchings, *Nat. Catal.*, 2019, **2**, 873–881.
34 X. Du, Y. Huang, X. Pan, B. Han, Y. Su, Q. Jiang, M. Li, H. Tang, G. Li and B. Qiao, *Nat. Commun.*, 2020, **11**, 5811.
35 C. T. Campbell, *Acc. Chem. Res.*, 2013, **46**, 1712–1719.
36 G. Bergeret and P. Gallezot, Particle Size and Dispersion Measurements, in *Handbook of Heterogeneous Catalysis*, ed. G. Ertl, H. Knözinger, F. Schüth and J. Weitkamp, 2008, DOI: **10.1002/9783527610044.hetcat0038**.
37 W. Zhang, H. Lin, Y. Wei, X. Zhou, Y. An, Y. Dai, Q. Niu, T. Lin and L. Zhong, *ACS Catal.*, 2024, **14**, 2409–2417.
38 J. Zhu Chen, J. Gao, P. R. Probus, W. Liu, X. Wu, E. C. Wegener, A. J. Kropf, D. Zemlyanov, G. Zhang, X. Yang and J. T. Miller, *Catal. Sci. Technol.*, 2020, **10**, 5973–5982.
39 J. Cai, Z. Yu, X. Fan and J. Li, *Molecules*, 2022, **27**(12), 3875.
40 J. L. Falconer and K. A. Magrini-Bair, *J. Catal.*, 1998, **179**, 171–178.
41 R. Rajalakshmi, G. Srividhya, C. Viswanathan and N. Ponpandian, *Appl. Catal., B*, 2023, **339**, 123089.
42 F. Giraud, C. Geantet, N. Guilhaume, S. Loridant, S. Gros, L. Porcheron, M. Kanniche and D. Bianchi, *Catal. Today*, 2021, **373**, 69.
43 B. A. Sexton, A. E. Hughes and K. Foger, *J. Catal.*, 1982, **77**, 85–93.